A Pitch Control Malfunction Analysis for Wind Turbines with PMSG and Full-Power Converters: Proportional Integral versus Fractional-Order Controllers

R. MELÍCIO

Department of Electromechanical Engineering
University of Beira Interior
R. Fonte do Lameiro, 6201-001 Covilha, Portugal

V. M. F. MENDES

Department of Electrical Engineering and Automation
Instituto Superior de Engenharia de Lisboa
R. Conselheiro Emídio Navarro, 1950-062 Lisbon, Portugal

J. P. S. CATALÃO

Department of Electromechanical Engineering
University of Beira Interior
R. Fonte do Lameiro, 6201-001 Covilha, Portugal

A transient analysis for two full-power converter wind turbines equipped with a permanent magnet synchronous generator (PMSG) is studied in this paper taking into consideration, as a new contribution to earlier studies, a pitch control malfunction. The two full-power converters considered are respectively a two-level and a multilevel converter. Moreover, a novel control strategy based on fractional-order controllers for the wind turbines is studied. Simulation results are presented, and conclusions are in favor of the novel control strategy, improving the quality of the energy injected into the electric grid.

Keywords fractional-order controller, pitch control malfunction, power converters, power quality, wind turbines

Manuscript received 14 April 2009

Address correspondence to J. P. S. Catalão, Department of Electromechanical Engineering, University of Beira Interior, R. Fonte do Lameiro, 6201-001 Covilha, Portugal. E-mail: catalao@ubi.pt

Nomenclature

u_0	Average wind speed.
u	Wind speed value with disturbance.
A_k	Magnitude of the eigenswing *k*.
ω_k	Eigenfrequency of the eigenswing *k*.
P_{tt}	Mechanical power of the turbine.
ρ	Air density.
R	Radius of the area covered by the blades.
c_p	Power coefficient.
ω_t	Rotor angular speed at the wind turbine.
θ	Pitch angle of the rotor blades.
λ	Tip speed ratio.
P_t	Mechanical power of the wind turbine disturbed by the mechanical eigenswings.
m	Order of the harmonic of a eigenswing.
g_{km}	Distribution of the m-order harmonic in the eigenswing *k*.
a_{km}	Normalized magnitude of g_{km}.
h_k	Modulation of eigenswing *k*.
φ_{km}	Phase of the m-order harmonic in the eigenswing *k*.
J_t	Moment of inertia for the rotor of the wind turbine.
T_t	Mechanical torque.
T_{dt}	Resistant torque in the wind turbine bearing.
T_{at}	Resistant torque in the hub and blades due to the viscosity of the airflow.
T_{ts}	Torsional stiffness torque.
ω_g	Rotor angular speed at the generator.
J_g	Moment of inertia for the rotor of the generator.
T_{dg}	Resistant torque in the generator bearing.
T_{ag}	Resistant torque due to the viscosity of the airflow in the generator.
T_g	Electric torque.
i_f	Equivalent rotor current.
M	Mutual inductance.
p	Number of pairs of poles.
i_d , i_q	Stator currents.
L_d , L_q	Stator inductances.
R_d , R_q	Stator resistances.
u_d , u_q	Stator voltages.

1. Introduction

The future growth of electrical power generation needs to be a mix of technologies including fossil fuels and hydro, nuclear, wind, and solar power [1]. In recent years there has been continuous growth of power generation from non-conventional energy sources [2]. Concerning these energy sources, wind power is becoming a priority in several countries, as nowadays occurs in Portugal.

In Portugal, the wind power goal foreseen for 2010 was established earlier by the government as 3750 MW, representing about 25% of the total installed capacity by 2010 [3]. But, this wind power goal has now been raised to 5100 MW. Hence, Portugal has one of the most ambitious goals in terms of wind power, and in 2006 was the second country in Europe with the highest wind power growth.

As the penetration level of wind power increases into the power systems, the overall performance of the electric grid will increasingly be affected by the characteristics of wind turbines. One of the major concerns related to the high penetration level of the wind turbines is the impact on power system stability [4]. Also, network operators have to ensure that consumer power quality is not deteriorated. Hence, the total harmonic distortion (THD) should be kept as low as possible, improving the quality of the energy injected into the electric grid [5].

Power-electronic converters have been developed for integrating wind power with the electric grid. The use of power-electronic converters allows not only for variable-speed operation of a wind turbine, but also for enhancement on power extraction [6]. In a recent overview of different wind generator systems [7], it is shown that variable speed conceptions equipped with power-electronic converts will continue to dominate and be very promising technologies for large wind farms.

In a variable-speed wind turbine with full-power converter, the wind turbine is directly connected to the generator and the generator is completely decoupled from the electric grid. Of all the generators used in wind turbines, the permanent magnet synchronous generator (PMSG) is the one with a significant advantage: it is stable and secure under normal operating conditions; and comparing with a wound synchronous generator, it is smaller and does not need a direct current power source for field excitation.

Non-fundamental harmonic emissions are recognized as a power quality disadvantage for modern variable-speed wind turbines. Understanding the harmonic behavior of variable-speed wind turbines is essential in order to analyze their effect on the electric grids where they are connected [8].

Variable-speed wind turbines usually employ active pitch control, where blade pitch angle increases reduce the captured of wind energy by reducing the angle of attack [9]. The pitch control may have an effect on the dynamical behavior of wind turbines, and research should be carried out in order to foresee its implications during different abnormal operating conditions. However, previous papers were mainly focused on the transient stability of variable-speed wind turbines at external grid faults [10, 11]. Grid code specifications in European countries require that wind turbines must be able to ride though grid disturbances that bring voltages down to very low levels [12]. Accordingly, great effort has been made to develop variable-speed wind turbines capable of supporting voltage/frequency and remain connected to the system during external grid faults [13, 14], but little attention has been given to the possibility of internal abnormal operating conditions, such as a pitch control malfunction.

This paper focuses on the analysis of the transient stability of wind turbines with PMSG and full-power converters, considering: (i) two different topologies for power-electronic converters, respectively two-level and multilevel converters, (ii) a novel fractional-order control strategy, which is compared with a classical integer-order control strategy, (iii) a pitch control malfunction. Simulation results for the pitch control malfunction ascertain the performance of wind turbines equipped with PMSG and two different topologies for the power-electronic converters, showing that the novel fractional-order control strategy improves the quality of the energy injected into the electric grid in what regards the THD.

2. Modeling

2.1. Wind Speed

The wind speed usually varies considerably and has a stochastic character. The wind speed variation can be modeled as a sum of harmonics with frequency range 0.1–10 Hz [15]:

$$u = u_0 \left[1 + \sum_k A_k \sin(\omega_k \, t) \right] \tag{1}$$

Hence, the physical wind turbine model is subjected to the disturbance given by the wind speed variation model [16].

2.2. Wind Turbine

The mechanical power of the turbine is given by:

$$P_{tt} = \frac{1}{2}\rho \pi R^2 u^3 c_p \tag{2}$$

The computation of the power coefficient requires the use of blade element theory and the knowledge of blade geometry. In this paper, the numerical approximation developed in [17] is followed, where the power coefficient is given by:

$$c_p(\lambda, \theta) = 0.73\left(\frac{151}{\lambda_i} - 0.58\theta - 0.002\theta^{2.14} - 13.2\right)e^{-\frac{18.4}{\lambda_i}} \tag{3}$$

$$\lambda_i = \frac{1}{\frac{1}{(\lambda - 0.02\theta)} - \frac{0.003}{(\theta^3 + 1)}} \tag{4}$$

The global maximum for the power coefficient is at null pitch angle and it is equal to:

$$c_{p\max}(\lambda_{opt}(0), 0) = 0.4412 \tag{5}$$

corresponding to an optimal tip ratio speed at null pitch angle equal to:

$$\lambda_{opt}(0) = 7.057 \tag{6}$$

Also, in order to achieve maximum power, the tip speed ratio at each pitch angle should be kept at the value corresponding to the global maximum for the power coefficient. Hence, the rotor angular speed at the wind turbine is as a function of the maximum mechanical power $P_{tt\max}$, given by:

$$\omega_t = \lambda_{opt}(\theta)\sqrt[3]{\frac{2\ P_{tt\max}}{\rho\ \pi\ R^5 c_{p\max}(\lambda_{opt}(\theta), \theta)}} \tag{7}$$

The maximum power point tracking (MPPT) algorithm is one of the key technologies of the power conversion system for effectively using the wind energy [18]. Nevertheless, gusts generated impact on the drive train and contribute significantly to fatigue loading due to rapid shaft torsional torque variations. Hence, a trade-off between operating at the optimum power coefficient and avowing rapid shaft torsional torque variations is important in practical implementations for reducing fatigue stresses [19]. This work is concerned with a transient analysis for wind turbines equipped with PMSG during a malfunction; to avoid excessive modeling only MPPT is used as in [6].

When regulating the wind system under the specification of maximum power, it must be taken into account that turbine power must never be higher than generator value for the rated power. Once generator rated power is reached at rated wind speed it must be limited. For variable-speed wind

turbines, a mechanical actuator is usually employed to change the pitch angle of the blades in order to reduce power coefficient and maintain the power at its rated value. When rated turbine speed is reached, control strategy must be changed so that a higher wind velocity no longer increases turbine speed but increases generated power until generator rated power; increases in rotor speed of about 10% are allowed during transients because of the slow pitch control response [20].

In order to model a pitch control malfunction, we consider that the pitch angle control of the blades imposes during a small time interval the position of wind gust on the blades, i.e., the blades go to the maximum pitch angle.

The maximum pitch angle $\theta_{\max} = 55^{\circ}$ is given for the minimum power coefficient, given by:

$$c_{p\min} = 0.0025 \tag{8}$$

corresponding to a tip speed ratio equal to:

$$\lambda_{\min} = 3.475 \tag{9}$$

The conversion of wind energy into mechanical energy over the rotor of a wind turbine is influenced by various forces acting on the blades and on the tower of the wind turbine (e.g. centrifugal, gravity and varying aerodynamic forces acting on blades, gyroscopic forces acting on the tower), introducing mechanical effects influencing the energy conversion. Those mechanical effects have been modeled by eigenswings mainly due to the following phenomena: asymmetry in the turbine, vortex tower interaction, and eigenswing in the blades. The mechanical power over the rotor of the wind turbine has been modeled, using the mechanical eigenswings, as a set of harmonic terms multiplied by the power associated with the energy capture from the wind by the blades, given by:

$$P_t = P_{tt}\left[1 + \sum_{k=1}^{3} A_k \left(\sum_{m=1}^{2} a_{km}\, g_{km}(t)\right) h_k(t)\right] \tag{10}$$

$$g_{km} = \sin\left(\int_0^t m\, \omega_k(t')\, dt' + \varphi_{km}\right) \tag{11}$$

The frequency range of the wind turbine model with mechanical eigenswings is from 0.1 to 10 Hz. The values used on (10) and (11) for the calculation of P_t, taken from [16], are given in Table 1.

"See Table 1 at the end of the manuscript".

2.3. Drive Train Model

A comparative study of wind turbine generator system using different drive train models [21] has shown that the two-mass model is suitable for transient stability analysis. Hence, a two-mass model for the drive train is considered in this paper. The configuration of the drive train model is shown in Figure 1.

"See Figure 1 at the end of the manuscript".

The equations for the two-mass model are based on the torsional version of the second law of Newton, deriving the state equation for the rotor angular speed at the wind turbine and for the rotor angular speed at the generator, respectively given by:

$$\frac{d\omega_t}{dt} = \frac{1}{J_t}\left(T_t - T_{dt} - T_{at} - T_{ts}\right) \tag{12}$$

$$\frac{d\omega_g}{dt} = \frac{1}{J_g}\left(T_{ts} - T_{dg} - T_{ag} - T_g\right) \tag{13}$$

2.4. PMSG

The model for the PMSG is the usual one, where the state equations for modeling the PMSG stator currents, using motor machine convention, are given by:

$$\frac{di_d}{dt} = \frac{1}{L_d}\left[u_d + p\,\omega_g\,L_q\,i_q - R_d\,i_d\right] \tag{14}$$

$$\frac{di_q}{dt} = \frac{1}{L_q}\left[u_q - p\,\omega_g\left(L_d\,i_d + M\,i_f\right) - R_q\,i_q\right] \tag{15}$$

In order to avoid demagnetization of permanent magnet in the PMSG, a null stator current $i_d = 0$ is imposed [22]. The electric power is given by:

$$P_g = [u_d \quad u_q \quad u_f][i_d \quad i_q \quad i_f]^T \tag{16}$$

2.5. Two-Level Converter

The two-level converter is an AC/DC/AC converter, with six unidirectional commanded insulated gate bipolar transistors (IGBTs) used as a rectifier, and with the same number of unidirectional commanded IGBTs used as an inverter. Each IGBT is indicated by its switching state S_{ij}. The index i with $i \in \{1,2\}$ identifies the IGBT. A group of two IGBTs linked to the same phase constitute a leg j of the converter. The index j with $j \in \{1,2,3\}$ identifies a leg for the rectifier and $j \in \{4,5,6\}$ identifies

the inverter one. The rectifier is connected between the PMSG and a capacitor bank. The inverter is connected between this capacitor bank and a second order filter, which in turn is connected to an electric grid. A three-phase active symmetrical circuit in series models the electric grid [23]. The phase currents injected in the electrical grid are modeled by the state equation given by:

$$\frac{di_{fj}}{dt} = \frac{1}{L_c}(u_{fj} - R_c\, i_{fj} - u_j) \qquad j = \{4,5,6\} \tag{17}$$

The configuration of the wind power system with two-level converter is shown in Figure 2.

"See Figure 2 at the end of the manuscript".

A switching variable γ_j of each leg j is used to identify the state of the IGBT i in the leg j of the converter. The switching variable of each leg j [24] is given by:

$$\gamma_j = \begin{cases} 1, \ (S_{1j} = 1 \ \text{and} \ S_{2j} = 0) \\ 0, \ (S_{1j} = 0 \ \text{and} \ S_{2j} = 1) \end{cases} \qquad j \in \{1, \ldots, 6\} \tag{18}$$

Hence, each switching variable depends on the conducting and blocking states of the IGBTs. The voltage v_{dc} is modeled by the state equation given by:

$$\frac{dv_{dc}}{dt} = \frac{1}{C}\left(\sum_{j=1}^{3}\gamma_j i_j - \sum_{j=4}^{6}\gamma_j i_j\right) \tag{19}$$

2.6. Multilevel Converter

The multilevel converter is an AC/DC/AC converter, with twelve unidirectional commanded IGBTs S_{ij} used as a rectifier, and with the same number of unidirectional commanded IGBTs used as an inverter. A group of four IGBTs linked to the same phase constitute a leg j of the converter. The rectifier is connected between the PMSG and a capacitor bank. The inverter is connected between this capacitor bank and a second order filter, which in turn is connected to an electric grid. Again, a three-phase active symmetrical circuit in series models the electric grid [25]. The phase currents injected in the electric grid are modeled by the state equation (17).

The configuration of the wind power system with multilevel converter is shown in Figure 3.

"See Figure 3 at the end of the manuscript".

The switching variable γ_j of each leg j is a function of the states S_{ij} of the converter. The index i with $i \in \{1,2,3,4\}$ identifies the IGBT. The index j with $j \in \{1,2,3\}$ identifies the leg for the rectifier

and $j \in \{4,5,6\}$ identifies the inverter one. The three valid conditions [26] for the switching variable of each leg j are given by:

$$\gamma_j = \begin{cases} 1, & (S_{1j} \text{ and } S_{2j}) = 1 \quad \text{and} \quad (S_{3j} \text{ or } S_{4j}) = 0 \\ 0, & (S_{2j} \text{ and } S_{3j}) = 1 \quad \text{and} \quad (S_{1j} \text{ or } S_{4j}) = 0 \\ -1, & (S_{3j} \text{ and } S_{4j}) = 1 \quad \text{and} \quad (S_{1j} \text{ or } S_{2j}) = 0 \end{cases} \qquad j \in \{1,\ldots,6\} \tag{20}$$

A switching variable Φ_{1j} is associated with the two upper IGBTs in each leg j (S_{1j} and S_{2j}), and also a switching variable Φ_{2j} is associated with the two lower IGBTs (S_{3j} and S_{4j}), respectively given by:

$$\Phi_{1j} = \frac{\gamma_j(1+\gamma_j)}{2} \quad ; \quad \Phi_{2j} = \frac{\gamma_j(1-\gamma_j)}{2} \qquad j \in \{1,\ldots,6\} \tag{21}$$

Hence, each switching variable depends only on the conducting and blocking states of the IGBTs. The voltage v_{dc} is the sum of the voltages v_{C1} and v_{C2} in the capacitor banks C_1 and C_2, modeled by the state equation given by:

$$\frac{dv_{dc}}{dt} = \frac{1}{C_1}\left(\sum_{j=1}^{3}\Phi_{1j}i_j - \sum_{j=4}^{6}\Phi_{1j}i_j\right) + \frac{1}{C_2}\left(\sum_{j=1}^{3}\Phi_{2j}i_j - \sum_{j=4}^{6}\Phi_{2j}i_j\right) \tag{22}$$

3. Control Strategy

3.1. Fractional-Order Controller

A novel control strategy based on fractional-order PI^{μ} controllers is studied for the variable-speed operation of wind turbines with PMSG and full-power converters. Fractional-order controllers are based on fractional calculus theory, which is a generalization of ordinary differentiation and integration to arbitrary (non-integer) order [27].

The fractional-order differentiator can be denoted by a general operator ${}_aD_t^{\mu}$ [28], given by:

$${}_aD_t^{\mu} = \begin{cases} \dfrac{d^{\mu}}{dt^{\mu}}, & \Re(\mu) > 0 \\ 1, & \Re(\mu) = 0 \\ \displaystyle\int_a^t (d\tau)^{-\mu}, & \Re(\mu) < 0 \end{cases} \tag{23}$$

The mathematical definition of fractional derivatives and integrals has been the subject of several descriptions. The most frequently encountered one is called Riemann–Liouville definition, in which the fractional-order integral is given by:

$$ {}_aD_t^{-\mu}\, f(t) = \frac{1}{\Gamma(\mu)} \int_a^t (t-\tau)^{\mu-1} f(\tau)\, d\tau \tag{24} $$

while the definition of fractional-order derivatives is:

$$ {}_aD_t^{\mu}\, f(t) = \frac{1}{\Gamma(n-\mu)} \frac{d^n}{dt^n} \left[\int_a^t \frac{f(\tau)}{(t-\tau)^{\mu-n+1}}\, d\tau \right] \tag{25} $$

where:

$$ \Gamma(x) \equiv \int_0^{\infty} y^{x-1}\, e^{-y}\, dy \tag{26} $$

is the Gamma function, a and t are the limits of the operation, and μ is the number identifying the fractional order. In this paper, μ is assumed as a real number that satisfies the restrictions $0 < \mu \leq 1$. Also, it is assumed that $a = 0$. The following convention is used: ${}_0D_t^{-\mu} \equiv D_t^{-\mu}$.

The differential equation of the fractional-order PI^{μ} controller, $0 < \mu < 1$, is given by:

$$ u(t) = K_p\, e(t) + K_i\, D_t^{-\mu}\, e(t) \tag{27} $$

where K_p is a proportional constant and K_i is an integration constant. In this paper, $\mu = 0.5$ and $\mu = 0.7$ are assumed. Taking $\mu = 1$ in (27), a classical PI controller is obtained. Hence, using Laplace transforms the transfer function of the fractional-order PI^{μ} and proportional integral PI controllers are respectively given by:

$$ G(s) = K_p + K_i\, s^{-\mu} \tag{28} $$

$$ G(s) = K_p + K_i\, s \tag{29} $$

3.2. Converters Control

Power converters are variable structure systems, because of the on/off switching of their IGBTs. As mentioned previously, the controllers used in the converters are respectively proportional integral and fractional-order PI^{μ} controllers. Pulse width modulation (PWM) by space vector modulation (SVM) associated with sliding mode is used for controlling the converters.

The sliding mode control strategy presents attractive features such as robustness to parametric uncertainties of the wind turbine and the generator as well as to electric grid disturbances [29].

Sliding mode controllers are particularly interesting in systems with variable structure, such as switching power converters, guaranteeing the choice of the most appropriate space vectors. Their aim is to let the system slide along a predefined sliding surface by changing the system structure.

The power semiconductors present physical limitations that have to be considered during design phase and during simulation study. Particularly, they cannot switch at infinite frequency. Also, for a finite value of the switching frequency, an error $e_{\alpha\beta}$ will exist between the reference value and the control value. In order to guarantee that the system slides along the sliding surface $S(e_{\alpha\beta},t)$, it has been proven that it is necessary to ensure that the state trajectory near the surfaces verifies the stability conditions [30] given by:

$$S(e_{\alpha\beta},t)\ \frac{dS(e_{\alpha\beta},t)}{dt}<0 \tag{30}$$

in practice a small error $\varepsilon>0$ for $S(e_{\alpha\beta},t)$ is allowed, due to power semiconductors switching only at finite frequency. Consequently, a switching strategy has to be considered, given by:

$$-\varepsilon<S(e_{\alpha\beta},t)<+\varepsilon \tag{31}$$

A practical implementation of the switching strategy considered in (31) could be accomplished by using hysteresis comparators.

The outputs of the hysteresis comparators are the integer variables $\sigma_{\alpha\beta}=(\sigma_\alpha,\sigma_\beta)$. For the two-level converter, σ_α and σ_β assume values in the set Ω given by:

$$\Omega\in\{-1,0,1\} \tag{32}$$

The appropriate vector selection in order to ensure stability for the two-level converter is shown in Table 2.

"See Table 2 at the end of the manuscript".

For the multilevel converter, σ_α and σ_β assume values in the set Ω given by:

$$\Omega\in\{-2,-1,0,1,2\} \tag{33}$$

In this control strategy, only when $v_{C1} \neq v_{C2}$ a new vector is selected. The appropriate vector selection in order to ensure stability for the multilevel converter is shown in Table 3, for $v_{C1} > v_{C2}$, and in Table 4, for $v_{C1} < v_{C2}$.

"See Table 3 at the end of the manuscript".

"See Table 4 at the end of the manuscript".

4. Simulation Results

The wind power system considered has a rated electric power of 900 kW. Table 5 summarizes the wind power system data.

"See Table 5 at the end of the manuscript".

The time horizon considered in the simulation is 4 s. The air density is 1.225 kg/m³. The wind speed model considered in this paper is:

$$u(t) = 15\left[1 + \sum_{k} A_k \sin(\omega_k\, t)\right] \qquad 0 \le t \le 4 \tag{34}$$

Figure 4 shows the profile of the wind speed.

"See Figure 4 at the end of the manuscript".

A pitch control malfunction is assumed to occur between 2 and 2.5 s, imposing a total cut-off on the capture of the energy from the wind by the blades.

The transient analysis of wind power systems, coupling electrical and mechanical subsystems where the temporal variations have different time scales, respectively, running fast and running slow, must be properly considered. Some times this consideration requires multirate integration schemes, for instance, multirate partitioned Runge-Kutta schemes [31]. Also, other strategies are possible for time stepping strategy [32].The mathematical model for the wind power system with the two-level and multilevel converters were implemented in Matlab/Simulink. After some tuning, a 4^{th}-order Runge-Kutta with a step size of 0.01 ms was used.

Figure 5 shows the mechanical power over the rotor of the wind turbine disturbed by the mechanical eigenswings, and the electric power of the generator.

"See Figure 5 at the end of the manuscript".

The pitch angle behavior is shown in Figure 6. The pitch angle is at 55º during pitch control malfunction, corresponding to the position of wind gust on the blades.

"See Figure 6 at the end of the manuscript".

The power coefficient behavior is shown in Figure 7. The power coefficient is at zero value during pitch control malfunction.

"See Figure 7 at the end of the manuscript".

The voltage v_{dc} for the two-level converter with a classical PI controller, fractional $PI^{0.5}$ and $PI^{0.7}$ controllers are shown in Figure 8. The voltage v_{dc} for the multilevel converter with a classical PI controller and fractional $PI^{0.5}$ and $PI^{0.7}$ controllers are shown in Figure 9.

"See Figure 8 at the end of the manuscript".

"See Figure 9 at the end of the manuscript".

Figure 8 and Figure 9 show that the classical PI controller responds with a larger drop on the DC voltage at the converter, during pitch control malfunction, in comparison with the fractional one. Nevertheless, the voltage drops are always inferior for the multilevel converter, in comparison with the ones for the two-level converter. A comparison between the maximum values for the DC voltage drops is shown in Table 6.

"See Table 6 at the end of the manuscript".

The voltage v_{dc} drops only 198.7 V during the pitch control malfunction with the multilevel converter and the fractional $PI^{0.7}$ controller. This is the best simulated case. While, the voltage v_{dc} drops almost 560 V during the pitch control malfunction with a two-level converter and a classical PI controller. This is the worst simulated case.

The output current with the fractional-order controller for the two-level converter is shown in Figure 10 and the one for the multilevel converter is shown in Figure 11.

"See Figure 10 at the end of the manuscript".

"See Figure 11 at the end of the manuscript".

A comparison between Figure 10 and Figure 11 shows that the output current ripple is lower with the multilevel converter than the one with the two-level converter.

The harmonic content of the current injected in the electric grid was evaluated using the THD, given by:

$$\text{THD}\ (\%) = 100\frac{\sqrt{\sum_{H=2}^{50} X_H^2}}{X_F} \tag{35}$$

where X_H is the root mean square (RMS) value of the non-fundamental harmonic component H, and X_F is the RMS value of the fundamental harmonic component.

The THD of the current injected in the electric grid with the fractional-order controller and a two-level converter is shown in Figure 12, while the one with the multilevel converter is shown in Figure 13.

"See Figure 12 at the end of the manuscript".

"See Figure 13 at the end of the manuscript".

Table 7 summarizes a comparison between the control strategies in what regards the THD.

"See Table 7 at the end of the manuscript".

The novel control strategy, based on fractional-order controllers, improves the performance in comparison with the classical *PI* control strategy. Moreover, the quality of the energy injected into the electric grid is improved, keeping the THD at a lower level. Accordingly, a minimum value of 0.03% is attained for the THD, considering the proposed fractional-order controller and multilevel converter.

5. Conclusions

The increased wind power penetration leads to new technical challenges, transient stability and power quality. In this paper, we present a model and a simulation study for variable speed wind turbines equipped with a PMSG and two different topologies for the power-electronic converters. The contributions of this paper are twofold: ascertaining the transient analysis at an internal fault, namely a pitch control malfunction, using two-level and multilevel converters; comparing a proportional integral strategy with a novel control strategy based on fractional-order controllers. The studied fractional-order controller for the variable speed operation of wind turbines equipped with a PMSG and multilevel converter improves the power quality, in comparison with a classical integer-order control strategy, in what regards the THD.

References

1. A. Abedini and A. Nasiri, "Output power smoothing for wind turbine permanent magnet synchronous generators using rotor inertia," *Electr. Power Compon. Syst.*, vol. 37, no. 1, pp. 1-19, Jan. 2009.
2. R.C. Bansal and T.S. Bhatti, "Reactive power control of autonomous wind-diesel hybrid power systems using Simulink," *Electr. Power Compon. Syst.*, vol. 35, no. 12, pp. 1345-1366, Dec. 2007.
3. A. Estanqueiro, R. Castro, P. Flores, J. Ricardo, M. Pinto, R. Rodrigues, and J. Peças Lopes, "How to prepare a power system for 15% wind energy penetration: the Portuguese case study," *Wind Energy*, vol. 11, pp. 75-84, Jan.-Feb. 2008.
4. N.R. Ullah and T. Thiringer, "Variable speed wind turbines for power system stability enhancement," *IEEE Trans. Energy Convers.*, vol. 22, pp. 52-60, Mar. 2007.
5. J. M. Carrasco, L.G. Franquelo, J.T. Bialasiewicz, E. Galvan, R.C.P. Guisado, A.M. Prats, J.I. Leon, and N. Moreno-Alfonso, " Power-electronic systems for the grid integration of renewable energy sources: A survey," *IEEE Trans. Ind. Electron.*, vol. 53, no. 4, pp. 1002-1016, Aug. 2006.
6. J.A. Baroudi, V. Dinavahi, and A.M. Knight, "A review of power converter topologies for wind generators," *Renew. Energy*, vol. 32, no. 14, pp. 2369-2385, Nov. 2007.
7. H. Li and Z. Chen, "Overview of different wind generator systems and their comparisons," *IET Renew. Power Gener.*, vol. 2, no. 2, pp. 123-138, Jun. 2008.
8. S. T. Tentzrakis and S. A. Papathanassiou, "An investigation of the harmonic emissions of wind turbines," *IEEE Trans. Energy Convers.*, vol. 22, pp. 150-158, Mar. 2007.
9. J.F. Conroy and R. Watson, "Low-voltage ride-through of a full converter wind turbine with permanent magnet generator," *IET Renew. Power Gener.*, vol. 1, no. 3, pp. 182-189, Sep. 2007.
10. C. Jauch, "Transient and dynamic control of a variable speed wind turbine with synchronous generator," *Wind Energy*, vol. 10, no. 3, pp. 247-269, Feb. 2007.
11. A.H. Kasem, E.F. El-Saadany, H.H. El-Tamaly, and M.A.A. Wahab, "An improved fault ride-through strategy for doubly fed induction generator-based wind turbines," *IET Renew. Power Gener.*, vol. 2, no. 4, pp. 201-214, Dec. 2008.
12. J.F. Conroy and R. Watson, "Aggregate modelling of wind farms containing full-converter wind turbine generators with permanent magnet synchronous machines: transient stability studies," *IET Renew. Power Gener.*, vol. 3, no. 1, pp. 39-52, Mar. 2009.

13. G. Ramtharan, J.B. Ekanayake, and N. Jenkins, "Frequency support from doubly fed induction generator wind turbines," *IET Renew. Power Gener.*, vol. 1, no. 1, pp. 3-9, Mar. 2007.
14. F.D. Kanellos and N.D. Hatziargyriou, "Control of variable speed wind turbines equipped with synchronous or doubly fed induction generators supplying islanded power systems," *IET Renew. Power Gener.*, vol. 3, no. 1, pp. 96-108, Mar. 2009.
15. Z.X. Xing, Q.L. Zheng, X.J. Yao, and Y.J. Jing, "Integration of large doubly-fed wind power generator system into grid," in Proc. 8th Int. Conf. Electrical Machines and Systems, pp. 1000-1004, Sep. 2005.
16. V. Akhmatov, H. Knudsen, and A.H. Nielsen, "Advanced simulation of windmills in the electric power supply," *Int. J. Electr. Power Energy Syst.*, vol. 22, pp. 421-434, Aug. 2000.
17. J.G. Slootweg, S.W.H. de Haan, H. Polinder, and W.L. Kling, "General model for representing variable speed wind turbines in power system dynamics simulations," *IEEE Trans. Power Syst.*, vol. 28, no. 1, pp. 144-151, Feb. 2003.
18. J. Hurng-Liahng, W. Kuen-Der, W. Jinn-Chang, and S. Jia-Min, "Simplified maximum power tracking method for the grid-connected wind power generation system," *Electr. Power Compon. Syst.*, vol. 36, no. 11, pp. 1208-1217, Nov. 2008.
19. E.B. Muhando, T. Senjyu, H. Kinjo, and T. Funabashi, "Augmented LQG controller for enhancement of online dynamic performance for WTG system," *Renew. Energy*, vol. 33, no. 8, pp. 1942-1952, Aug. 2008.
20. M. Chinchilla, S. Arnaltes, and J.C. Burgos, "Control of permanent-magnet generators applied to variable-speed wind energy systems connected to the grid," *IEEE Trans. Energy Convers.*, vol. 21, no. 1, pp. 130-135, Mar. 2006.
21. S.M. Muyeen, M. Hasan Ali, R. Takahashi, T. Murata, J. Tamura, Y. Tomaki, A. Sakahara, and E. Sasano, "Transient stability analysis of grid connected wind turbine generator system considering multi-mass shaft modeling," *Electr. Power Compon. Syst.*, vol. 34, no. 10, pp. 1121-1138, Oct. 2006.
22. T. Senjyu, S. Tamaki, N. Urasaki, and K. Uezato, "Wind velocity and position sensorless operation for PMSG wind generator," in Proc. 5th Int. Conf. on Power Electronics and Drive Systems 2003, pp. 787-792, Nov. 2003.
23. R. Melício, V.M.F. Mendes, and J.P.S. Catalão, "Two-level and multilevel converters for wind energy systems: a comparative study," in Proc. 13th Int. Power Electron. Motion Control Conf., pp. 1682-1687, Sep. 2008.

24. J.F. Silva, and S.F. Pinto, *Control methods for switching power converters*, Rashid, M.H. (Ed.): "Power Electronics Handbook" (Academic Press, 2007), pp. 935-998.

25. R. Melício, V.M.F. Mendes, and J.P.S. Catalão, "Evaluating power quality in wind power generation systems with two-level and multi-level converters," in Proc. 6th Mediterr. Conf. and Exhib. on Power Gener. Transm. Distrib. and Energy Convers., Nov. 2008.

26. J.D. Barros, and J.F. Silva, "Optimal predictive control of three-phase NPC multilevel converter for power quality applications," *IEEE Trans. Ind. Electron.*, vol. 55, no. 10, pp. 3670-3681, Oct. 2008.

27. I. Podlubny, "Fractional-order systems and PI-lambda-D-mu-controllers," *IEEE Trans. Autom. Control*, vol. 44, no. 1, pp. 208-214, Jan. 1999.

28. A.J. Calderón, B.M. Vinagre, and V. Feliu, "Fractional order control strategies for power electronic buck converters," *Signal Processing*, vol. 86, no. 10, pp. 2803-2819, Mar. 2006.

29. B. Beltran, T. Ahmed-Ali, and M.E.H. Benbouzid, "Sliding mode power control of variable-speed wind energy conversion systems," *IEEE Trans. Energy Convers.*, vol. 23, no. 2, pp. 551-558, Jun. 2008.

30. S. Pinto, and J. Silva, "Sliding mode direct control of matrix converters," *IET Electr. Power Appl.*, vol. 1, no. 3, pp. 439-448, May 2007.

31. M. Günther, A. Kværnø, and P. Rentrop, "Multirate partitioned Runge-Kutta methods," *BIT Numerical Mathematics*, vol. 41, no. 1, pp. 504-514, Jun. 2001.

32. V. Savecenco, W. Hundsdorfer, and J.G. Verwer, "A multirate time stepping strategy for stiff ordinary differential equations," *BIT Numerical Mathematics*, vol. 47, no. 1, pp. 137-155, Mar. 2007.

Figure captions

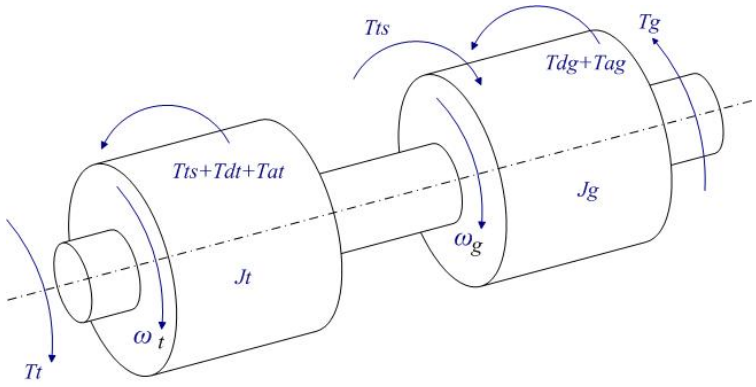

Figure 1. Configuration of the drive train model.

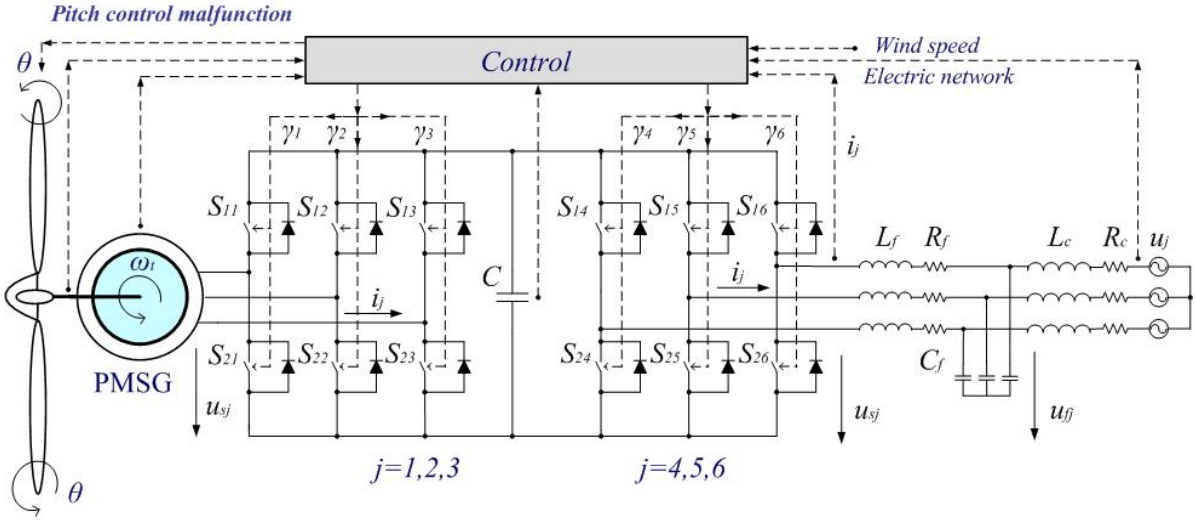

Figure 2. Wind power system with two-level converter.

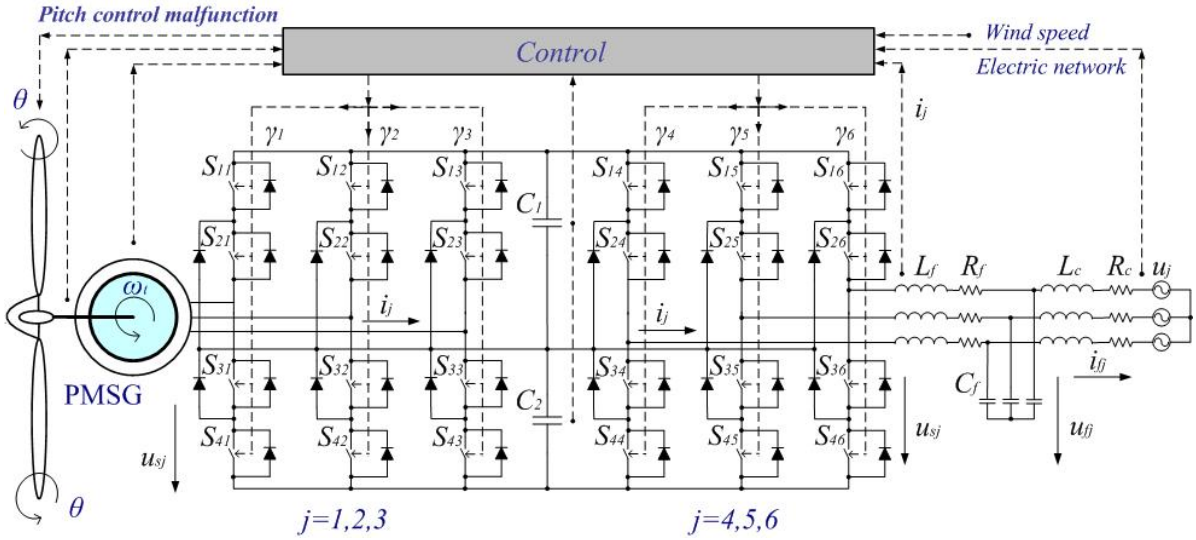

Figure 3. Wind power system with multilevel converter.

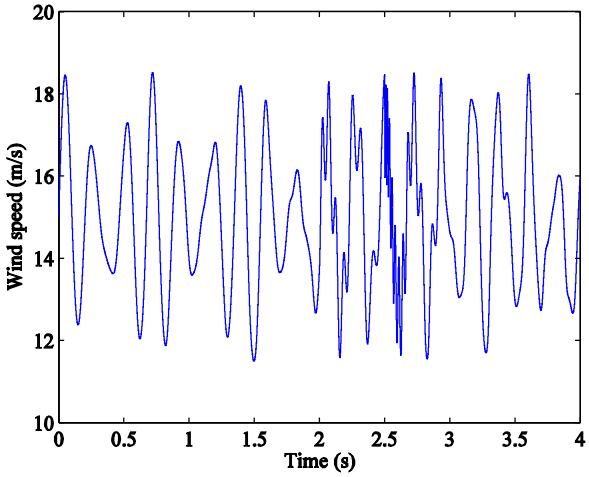

Figure 4. Profile of the wind speed.

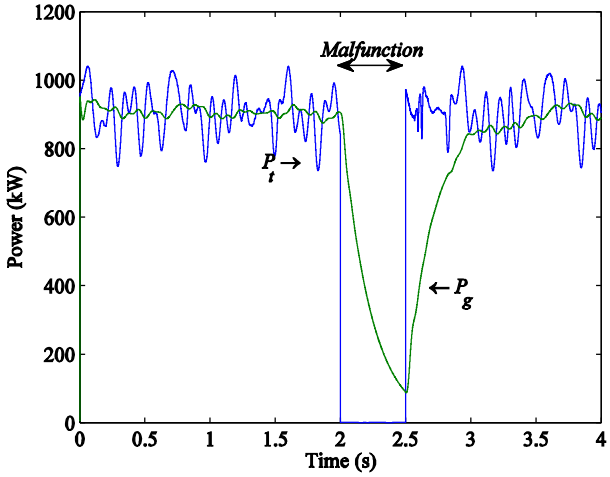

Figure 5. Mechanical power over the rotor and electric power.

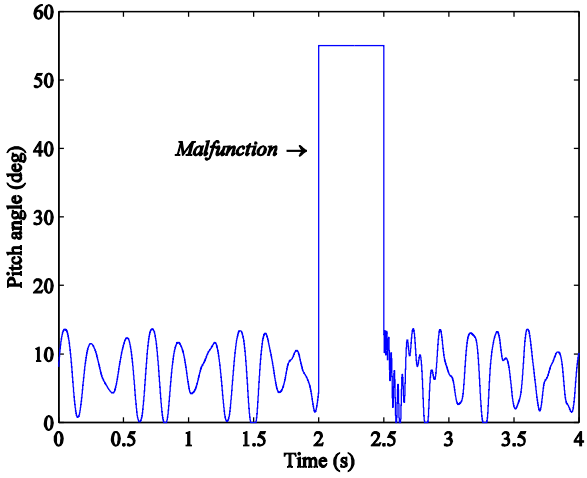

Figure 6. Pitch angle variation.

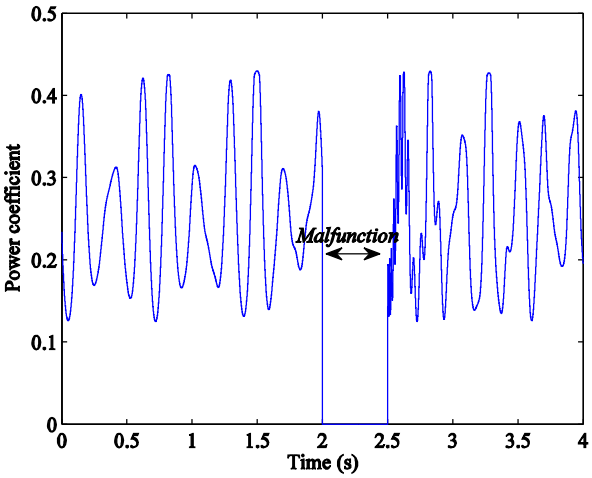

Figure 7. Power coefficient variation.

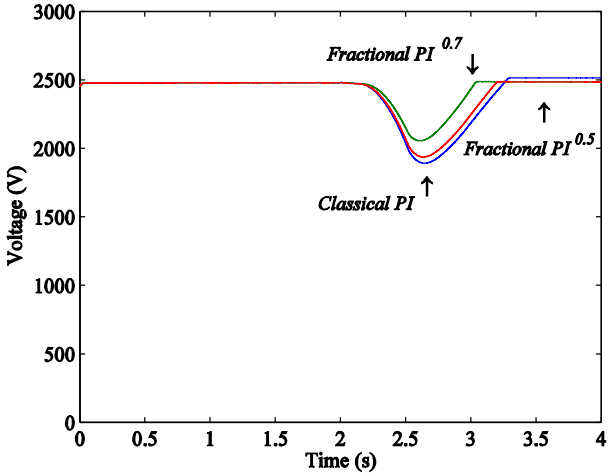

Figure 8. Voltage v_{dc} for the two-level converter, considering each controller.

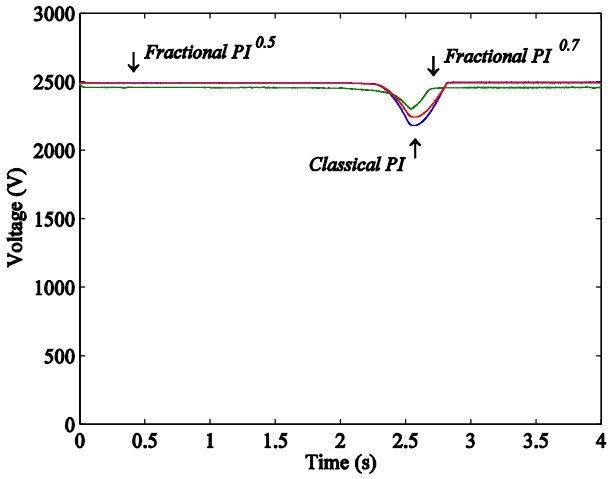

Figure 9. Voltage v_{dc} for the multilevel converter, considering each controller.

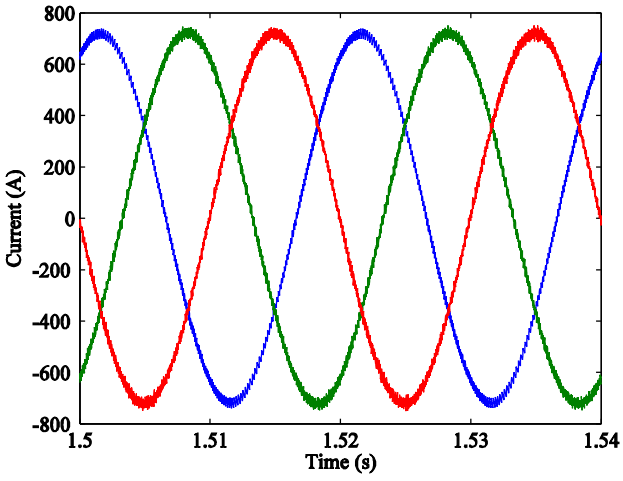

Figure 10. Output current of the two-level converter.

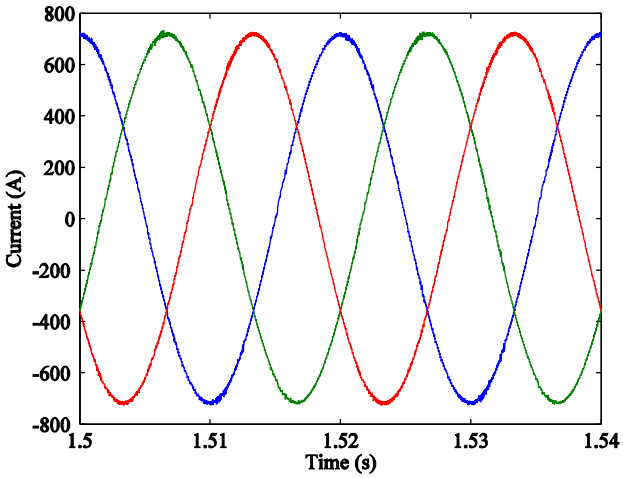

Figure 11. Output current of the multilevel converter.

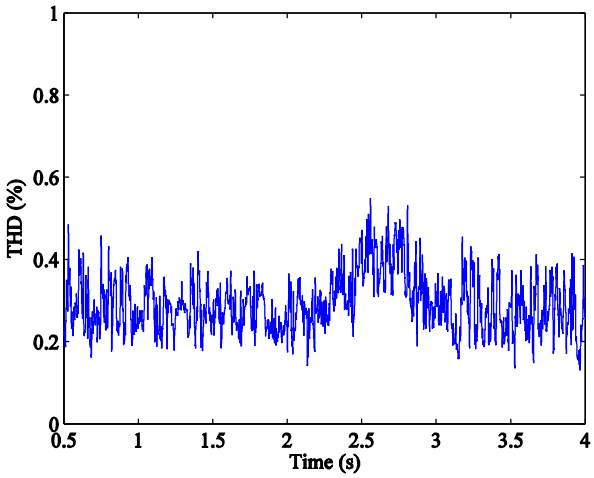

Figure 12. THD of the current injected in the electric grid with the two-level converter.

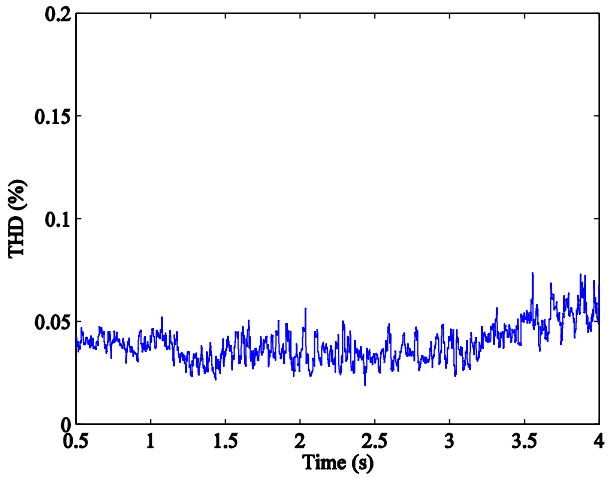

Figure 13. THD of the current injected in the electric grid with the multilevel converter.

Tables

Table 1
Mechanical eigenswings excited in the wind turbine

k	Source	A_k	ω_k [rad/s]	h_k	m	a_{km}	φ_{km}
1	Asymmetry	0.01	ω_t	1	1	4/5	0
					2	1/5	$\pi/2$
2	Vortex tower interaction	0.08	$3\,\omega_t$	1	1	1/2	0
					2	1/2	$\pi/2$
3	Blades	0.15	$9\,\pi$	$1/2\,(g_{11}+g_{21})$	1	1	0

Table 2
Output voltage vectors selection for the two-level converter

$\sigma_\beta \setminus \sigma_\alpha$	-1	0	1
-1	4	4;5	5
0	6	0;7	1
1	2	3;2	3

Table 3
Output voltage vectors selection for the multilevel converter, for $v_{C1} > v_{C2}$

$\sigma_\beta \setminus \sigma_\alpha$	-2	-1	0	1	2
-2	25	25	12	7	7
-1	24	13	13;6	6	8
0	19	18	1;14;27	5	9
1	20	17	17;2	2	4
2	21	21	16	3	3

Table 4
Output voltage vectors selection for the multilevel converter, for $v_{C1} < v_{C2}$

$\sigma_\beta \setminus \sigma_\alpha$	-2	-1	0	1	2
-2	25	25	12	7	7
-1	24	26	26;11	11	8
0	19	23	1;14;27	10	9
1	20	22	22;15	15	4
2	21	21	16	3	3

Table 5
Wind power system data

Turbine moment of inertia	2500.10³ kgm²
Turbine rotor diameter	49 m
Tip speed	17.64-81.04 m/s
Rotor speed	6.9-31.6 rpm
Generator rated power	900 kW
Generator moment of inertia	100.10³ kgm²

Table 6
Capacitor voltage drop during pitch control malfunction

Controller	v_{dc} (V)	
	Wind power system with two-level converter	Wind power system with multilevel converter
Classical PI	559.1	320.4
Fractional $PI^{0.5}$	513.7	258.8
Fractional $PI^{0.7}$	395.5	198.7

Table 7
THD of the current injected in the electric grid

Controller	THD (%)	
	Wind power system with two-level converter	Wind power system with multilevel converter
Classical PI	0.46	0.08
Fractional $PI^{0.5}$	0.29	0.05
Fractional $PI^{0.7}$	0.17	0.03

About the authors

R. Melício received the M.Sc. degree from the Instituto Superior Técnico, Lisbon, Portugal, in 2004. He is currently a Ph.D. student at the University of Beira Interior, Covilha, Portugal, in collaboration with the Instituto Superior de Engenharia de Lisboa, Lisbon, Portugal. His research interests include power electronic converters, power quality, and wind energy systems.

V. M. F. Mendes received the M.Sc. and Ph.D. degrees from the Instituto Superior Técnico, Lisbon, Portugal, in 1987 and 1994, respectively. He is currently a Coordinator Professor with Aggregation at the Instituto Superior de Engenharia de Lisboa, Lisbon, Portugal. His research interests include hydrothermal scheduling, optimization theory and its applications, and renewable energies. He is the author or co-author of more than 110 scientific papers presented at international conferences or published in reviewed journals.

J. P. S. Catalão received the M.Sc. degree from the Instituto Superior Técnico, Lisbon, Portugal, in 2003 and the Ph.D. degree from the University of Beira Interior, Covilha, Portugal, in 2007. He is an IEEE and IET Member. He is currently an Assistant Professor at the University of Beira Interior. His research interests include hydro scheduling, unit commitment, price forecasting, wind energy systems, and electricity markets. He is the author or co-author of more than 70 scientific papers presented at international conferences or published in reviewed journals. Dr. Catalão is an Associate Editor for the *International Journal of Power and Energy Systems*, and a Member of the Editorial Board of *Electric Power Components & Systems*.